Summer 2014

Aspen simulation of furfural and hydroxymethylfurfural production from biomass

Zachary Daniel King

ASPEN SIMULATION OF FURFURAL AND HYDROXYMETHYLFURFURAL PRODUCTION FROM BIOMASS

by

ZACHARY DANIEL KING

A THESIS

Presented to the Faculty of the Graduate School of the

MISSOURI UNIVERSITY OF SCIENCE AND TECHNOLOGY

In Partial Fulfillment of the Requirements for the Degree

MASTER OF SCIENCE IN CHEMICAL ENGINEERING

2014

Approved by:

Dr. Neil L. Book, Advisor
Dr. Muthanna H. Al-Dahhan
Dr. Joseph Smith

ABSTRACT

Biomass field liquefaction is a concept where green biomass is chemically treated to produce organic liquids using small-scale equipment in the field. If liquefaction occurs as the crop is harvested, the energy requirements for growing the biomass can be charged to the crop as if the biomass were left in the field. The energy in the organic liquid product is available at the expense of the energy required by the process. A simplified process was simulated using ASPEN to assess the energy production feasibility.

Acid catalyzed liquefaction of cellulose and hemicellulose solids produces furfural and hydroxymethylfurfural (HMF). The simulation assumed furfural from xylans and HMF from hexosans were the only organic products. Reaction rate was regressed from published data. Complete physical properties were estimated for HMF using group contribution methods (Marrero-Pardillo, critical properties; Benson, ideal gas heat capacity and standard heat of formation; UNIFAC, vapor-liquid-liquid equilibrium).

Two figures of merit were determined over a range of process temperatures, residence times, and feed compositions (xylan, hexosan, and a mixture representative of corn stover). Maximum energy recovery ratio was nearly 2/3 and represents the ratio of combustion energy in the organic liquid product minus energy required for the reactor to biomass feed combustion energy. This value occurred at short residence time, desirable for field liquefaction. The product to process energy ratio is the ratio of the combustion energy in the organic liquid product to the process energy requirements. The 9:1 maximum occurred with low temperature and high conversion (long residence time). The value was greater than 7:1 for high temperature and conversion (short residence time), which compares favorably with the enzymatic ethanol biomass reported value of 2.61:1.

ACKNOWLEDGMENTS

The author thanks Dr. Neil Book for his insight, assistance and patience, Justin Cobb for his work on the properties on hydroxymethylfurfural, committee member Dr. Oliver Sitton for his knowledge of ASPEN, and committee members Dr. Muthanna Al-Dahhan and Dr. Joseph Smith for their participation.

TABLE OF CONTENTS

LIST OF ILLUSTRATIONS

LIST OF TABLES

1. INTRODUCTION

The patent, A Process for the Liquefaction of Lignocellulosic Material (Petrus and Voss, 2005), describes a process for the solvent liquefaction of lignocellulosic residues. The process achieves high liquefaction fractions in short residence times. The short residence times create the potential for performing the liquefaction in the field with small-scale equipment on green (wet) residues and transporting the liquid product to a large-scale refinery where the crude product is converted to fuels and/or chemicals. The potential advantages of field liquefaction are:

1) Single-pass harvesting
2) Transport and storage of liquid products
3) Enhanced revenue from co-product residues.

1.1. AGRICULTURAL RESIDUES

Harvesters, such as combines, harvest much of the plant and then separate the grain from the biomass which is returned to the field. After field drying, a second pass is required to bale the residues. Since the residues are a distributed resource and produced seasonally but processed continuously at large-scale facilities, transportation and storage costs are significant. The spontaneous combustion of wet residues and the natural degradation of residues in storage complicate the problem.

Adding liquefaction equipment to the harvester has the potential to allow single-pass harvesting of both grain and plant residue. Farms and grain elevators could add liquid storage facilities to take advantage of off-season collection price increments as is done with grain. Pipeline systems from elevators or other liquid storage facilities to large-scale refineries provide inexpensive solutions for large-scale transportation of liquids. Most importantly, the farmer realizes additional revenues with very small incremental costs (a tank truck would be required for transportation of liquid products).

1.2. FOREST RESIDUES

The logs produced from a tree represent a small fraction of the total biomass. Leaves, branches and tops are left in the forest. Small-scale liquefaction equipment that converts the residues to a liquid product that can be pumped from the forest to a tank truck represents the potential to coproduce value from the residues.

1.3. ENERGY PRODUCTION EFFICIENCY

Studies on biomass and petrochemical processes for energy employ a variety of comparison strategies. These often reflect the scope of the analysis as well as assumptions made and insure consistent and equitable comparison between renewable biomass and fossil fuel processes. At one extreme, a comprehensive life cycle analysis of energy inputs is employed. On the other, only the process by which feedstock is converted to product is used. The former must include the later and thus requires additional assumptions. Further when biomass such as corn stover and not grain, for which the crop was grown, is used as a feedstock, the energy and monetary costs associated with growing the crop are shared. Assigning value for these co-products is another important parameter in energy production efficiency comparisons.

There has been considerable controversy over the amount of net energy that is obtained from ethanol produced from grain. Pimental and Patzek claim that more energy is expended in production, harvesting and converting the grain to ethanol than is derived from its combustion as a fuel (2005). Graboski refutes Pimentel’s claims, and, based on a different set of assumptions, indicates that there is a positive net energy production from grain-derived ethanol (2002). However, the ratio of available combustion energy to production energy consumed was, at best, approximately 5:4. Thus, a 100,000-gallon per year grain ethanol plant requires the consumption of the equivalent of 80,000 gallons per year having a net energy production of only 20,000 gallons per year. This is in stark contrast to the petroleum-derived fuels that consume about 7% (Graboski, 2002) of the available energy (14:1 ratio) in production. Lorenz et al. estimate that the product to process energy ratio is approximately 2.62:1 for ethanol derived from enzymatic hydrolysis of lignocellulosic residues. The estimates for the enzymatic hydrolysis process are based on second-pass harvesting of field-dried residues and assume that conversion efficiencies obtained from small-scale equipment with uniform feedstocks will be obtained at large scale with seasonal feedstocks that vary widely in composition.

1.4. PRODUCTION OF FURFURALS

A method of producing furfurals is to hydrolyze the biomass into the constituent sugars and then dehydrate. Both reactions are acid catalyzed.

$$\underset{\text{Celluloses}}{-C_n\left(H_2O\right)_{n-1}-} + H_2O \longrightarrow \underset{\text{Sugars}}{C_n\left(H_2O\right)_n} \longrightarrow \underset{\text{Furfurals}}{C_n\left(H_2O\right)_{n-3}} + 3\,H_2O$$

The hemicellulose fraction of the biomass contains a large percentage of xylans which dehydrate to furfural. The cellulose fraction of the biomass is composed of hexosans that dehydrate to hydroxymethylfurfural (HMF).

1.5. THERMODYNAMIC COMPARISON

Various processes are available for converting biomass to both energy and feedstocks for further processing including; synthesis gas (SynGas, H_2 and CO), methane, ethanol and furfurals. Two factors that can describe the thermodynamics of each of these processes is the enthalpy of reaction to create the products and the chemical energy embodied by the products. If complete combustion is assumed in all cases, the sum of the process energy and combustion energy must be the same for each process for thermodynamic consistency.

Figure 1.1 and Figure 1.2 show these thermodynamic relationships starting with both xylan, a pentosan, and cellulose, a hexosan for six routes from the feed to complete combustion. The molar quantities have multipliers so that both processes result in the same molar quantities of combustion products. See Appendix B for results of simulations. Exothermic reactions may offer energy to carry out the process but represent a net loss from feedstock to product. Endothermic reactions represent a necessary input to the process in the form of energy or using some of the feed to drive the process and generally require a high temperature process. However, the energy input in the conversion process is recovered in the combustion of the fuel. The most appealing processes will neither be highly endothermic or exothermic. The conversion of xylans and hexosans to furfurals in very nearly athermal. Thus, energy expended in the furfural conversion process is lost and cannot be recovered during combustion.

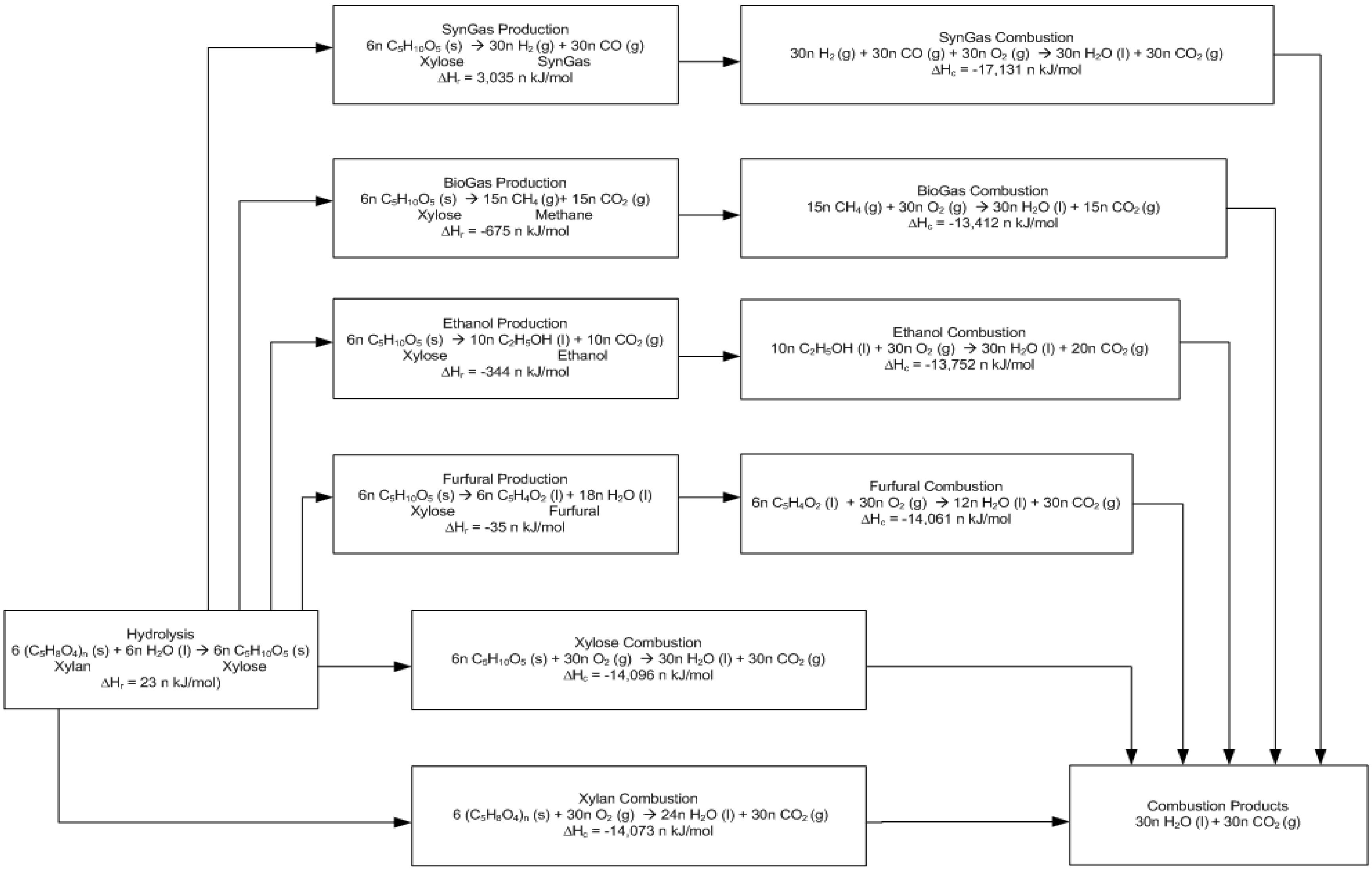

Figure 1.1 Chemical Pathways for the Combustion of Xylan

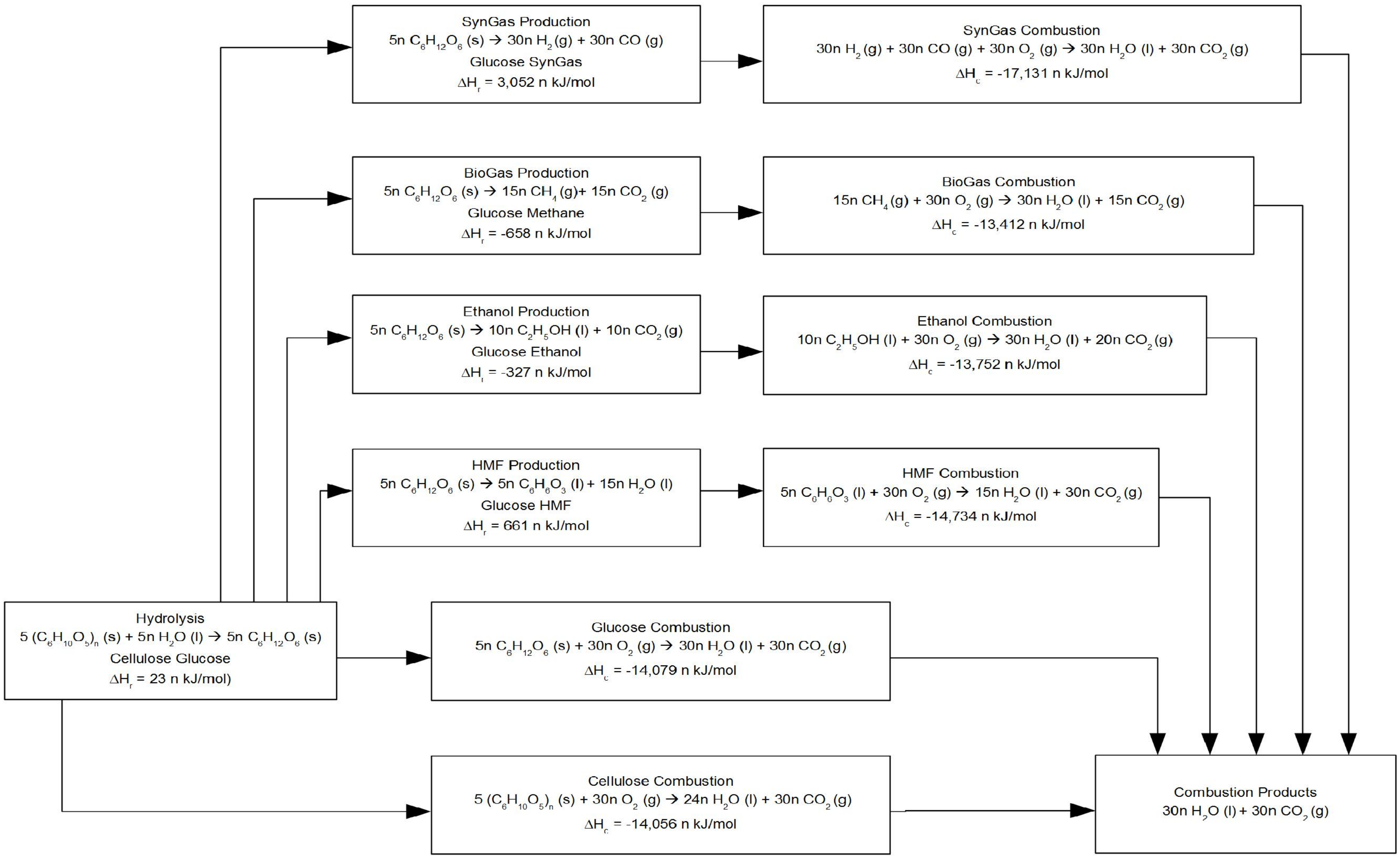

Figure 1.2 Chemical Pathways for the Combustion of Cellulose

1.6. SIMULATION OF THE SOLVENT LIQUEFACTION PROCESS

A process flow diagram for solvent liquefaction of biomass is given in Figure 1.3.

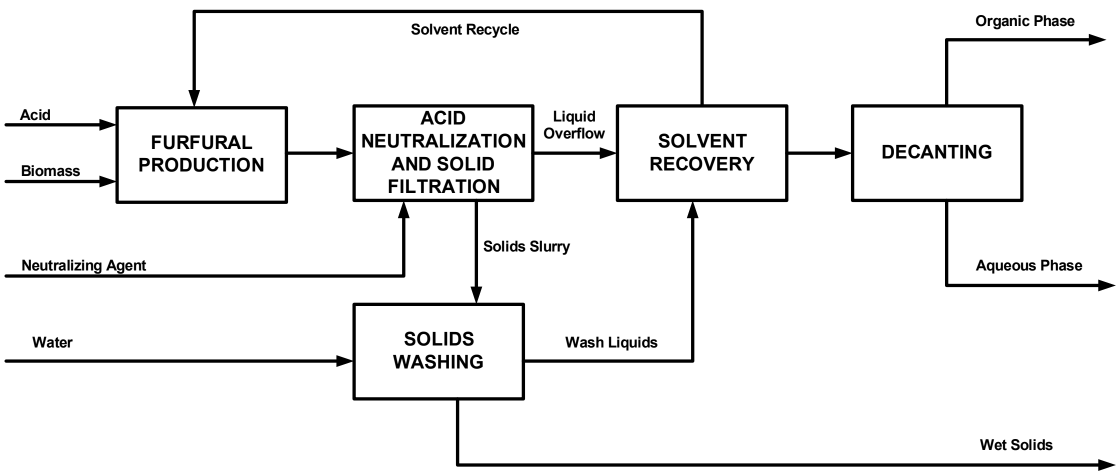

Figure 1.3 Solvent Liquefaction Process for Biomass

Biomass, acid solution, and solvent are fed to a reactor in which the cellulose and hemicellulose fractions of the biomass are converted to organic liquids. A neutralizing agent is added to the product of the reactor to convert the acid to a solid precipitate (such as lime addition to sulfuric acid to form gypsum). The solids (precipitate and unreacted solids) are filtered and washed with water to recover entrapped solvent and organic liquids. The solvent is recovered from the overflows from the filter and recycled. Upon cooling to atmospheric conditions, two liquid phases form that can be decanted.

The patent used levulinic acid and gamma valerolactone as the liquefaction solvent. However, a claim was made for a family of compounds (containing these two compounds) that could serve as the solvent. For the field liquefaction, high solvent recoveries for recycle are necessary so that quantities of makeup solvent are minimal. A solvent, perhaps from this family, but with a moiety that is effective at liquefaction, unaffected by the neutralization process, and easily recovered will be required. The washed solids are returned to the soil to satisfy the soil conservation requirements.

A simulation of a simplified version of the solvent liquefaction process has been performed to assess energy production efficiency. The process flow diagram for the simulation is given in Figure 1.4.

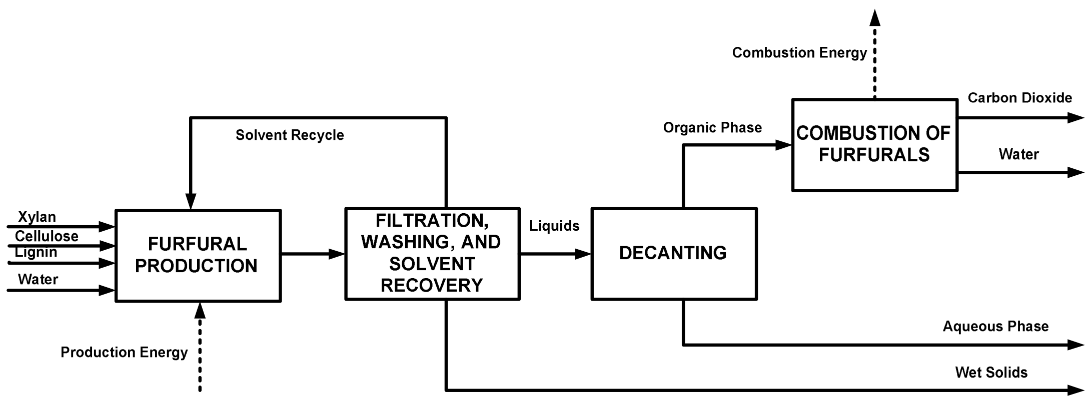

Figure 1.4 Process Flow Diagram for Simulation

It is assumed that an acid/solvent combination exists that converts xylans to furfural and cellulose to HMF. The feedstock is taken to be a green residue that is modeled as a moist solid composed of cellulose and hemicelluloses. The patent achieves high solids liquefaction percentages that indicate lignin is also liquefied. The chemical products of lignin liquefaction are unknown so the solid feed is taken to be free of lignin. The cellulose is assumed to hydrolize to glucose and then dehydrate to hydroxymethylfurfural (HMF). The hemicellulose fraction is assumed to be xylan that hydrolizes to xylose and then dehydrates to furfural.

Water, furfural, and HMF can form immiscible liquid phases: an aqueous or water-rich phase that is predominantly water and an organic or furfural-rich phase that is largely furfurals. The energy efficiency of the process is measured using a figure of merit defined as the ratio of the combustion energy in the HMF and furfural in the organic phase minus the process energy requirement to the combustion energy in the cellulose and hemicellulose in the feedstock. The figure of merit is determined for wet feedstocks of varying composition, process temperature and residence times in order to assess the energy production potential of the solvent liquefaction process.

2. REVIEW OF THE LITERATURE

2.1. PHYSICAL PROPERTIES

2.1.1. Minimum Physical Properties Required by ASPEN. The ASPEN process simulator requires certain physical properties dependent on the calculation method selected. In this simulation UNIFAC is used to predict the vapor-liquid-liquid equilibrium of the furfurals and water. For these compounds involved in the vapor-liquid-liquid equilibrium calculations a complete set of physical properties are required. In ASPEN this will depend on the calculation route used. For this simulation; critical temperature, critical pressure, ideal gas heat of formation, vapor pressure, ideal gas heat capacity, heat of vaporization, and liquid density are required. For solids, xylan and cellulose, which are not involved in the vapor-liquid-liquid equilibrium only heat capacity and density are required.

2.1.2. Properties of HMF. Furfural is a commercial solvent and precursor chemical so its physical properties have been measured. Hydroxymethylfurfural (HMF) is not a common commercial product and many of its properties have been estimated. The complete list of physical properties used in the simulation can be found in Table 2.1.

Hydroxymethylfurfural (HMF) is the common name for 5-hydroxymethyl-2-furancarboxaldehyde, (CAS Registry Number 67-47-0). HMF is formed by the dehydration of glucose in the presence of an acid catalyst.

$$C_6H_{12}O_6 \xrightarrow{\text{Acid}} C_6H_6O_3 + 3\,H_2O$$

Other common names are: 2-furaldehyde, 5-(hydroxymethyl)-; 5-hydrxoymethylfurfural; hydroxymethylfurfurole; HMF; 5-(hyddroxymethyl)furfurole; 5-(hydroxymethyl)-2-formylfuran;
5-(hydroxymethyl)-2-furaldehyde; 5-(hydroxymethyl)-2-furancarbonal; 5-(hydroxymethyl)-2-furfural;
5-(hydroxymethyl)-2-furfuraldehyde; 5-(hydroxymethyl)furan-2-aldehyde; 5-(hydroxymethyl)furfural;

5-hydroxymethylfuraldehyde; 5-oxymethylfurfurole; 5-hydroxymethylfurfuraldehyde; 5-hydroxymethyl-2-furancarbaldehyde; hydroxymethylfurfuraldehyde; 5-(hydroxymethyl)-2-furancarboxaldehyde; and
2-hydroxymethyl-5-furfural; 5-(hydroxymethyl)-2-furfural). The chemical structure is:

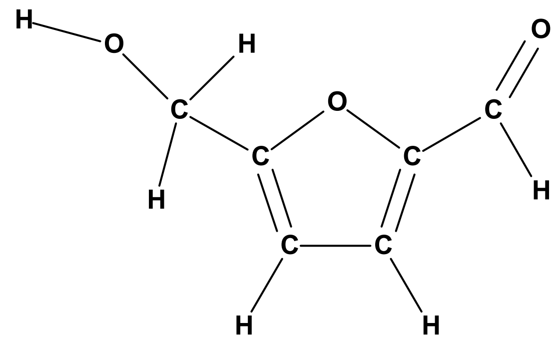

The base chemical structure is a furan ring. The molecular mass is 126.11 g/mol.

Table 2.1 Physical Properties of HMF

Property	ASPEN Property	Units	Value	See Section
Molecular Weight	MW		126.11	
Critical Temperature	TC	K	787.9	2.1.2.2
Critical Pressure	PC	bar	56.4	2.1.2.2
Boiling Point		K	564	2.1.2.2
Ideal Gas Heat of Formation	DHFORM	J/Kmole	-277200000	2.1.2.5
Ideal Gas Energy of Formation	DGFORM	J/Kmole	-186000000	2.1.2.5
Vapor Pressure	PLXANT/1 PLXANT/2	Pascal	25.67 -7977	2.1.2.3
Ideal Gas Heat Capacity	CPIG/1 CPIG/2	J/Kmole K	-5234.35936 535.854217	2.1.2.5
Liquid Molar Volume	RKTZRA	cum/kmol	0.0621	2.1.2.4

2.1.2.1 Chemicals with similar structure. A number of chemical species have a structure that is similar to HMF and have published data. The methods used to estimate the physical properties of HMF were used on these compounds to confirm the accuracy of the methods.

- **Furfural**

The chemical structure of 2-furancarboxaldehyde (furfural; 2-furaldehyde; α-furole; artificial ant oil; fural; furaldehyde; furale; furancarbonal; furfuraldehyde; furfurole; furfurylaldehyde; furole; pyromucic aldehyde; 2-formylfuran; 2-furanaldehyde; 2-furancarbonal; 2-furfural; 2-furfuraldehyde; 2-furylaldehyde; furol; 2-furylmethanal; artificial oil of ants; furfurale; furfurol; NCI-C56177; 2-furil-metanale; 2-furankarbaldehyd; furfuralu; RCRA waste number U125; UN 1199; 2-furylaldehyde xypropane;
2-furylcarboxaldehyde; cyclic aldehyde; QO furfural; 2-furancarboxyaldehyde; furan-2-aldehyde; furan-2-carbaldehyde; furancarboxaldehyde) is:

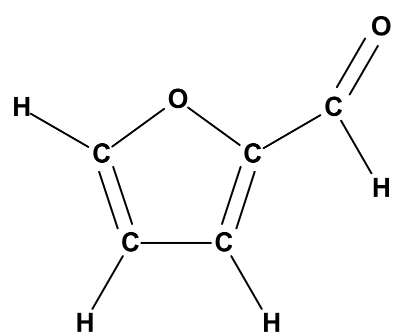

The normal boiling point is 434.7 ± 0.4 K as reported in the NIST Chemistry WebBook (Brown and Stein & Thermodynamics Research Center). The molecular mass is 96.0841 g/mol.

- **Furan**

The chemical structure of furan (divinylene oxide; furfuran; oxacyclopentadiene; oxole; tetrole; furane; furfurane; NCI-C56202; RCRA waste number U124; UN 2389; QO furan) is:

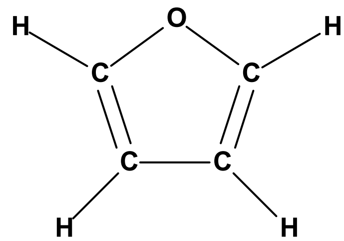

The normal boiling point is 304.7 ± 0.6 K as reported in the NIST Chemistry WebBook (Brown and Stein & Thermodynamics Research Center). Poling et al. report the boiling point as 304.44 K. The molecular mass is 68.0740 g/mol.

- **<u>Methylfuran (MF)</u>**

The chemical structure of 2-methylfuran is:

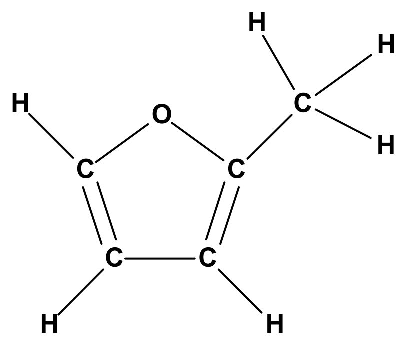

The normal boiling point is 337. ± 1. K as reported in the NIST Chemistry WebBook (Brown and Stein, Thermodynamics Research Center). Poling et al. report the boiling point as 337.87 K. The molecular mass is 82.1005 g/mol.

- **<u>Tetrahydrofuran (THF)</u>**

The chemical structure of tetrahydrofuran (butane α,δ-oxide; butane, 1,4-epoxy-; cyclotetramethylene oxide; furanidine; oxacyclopentane; oxolane; tetramethylene oxide; THF; hydrofuran; tetrahydrofuraan; tetrahydrofuranne; tetraidrofurano; NCI-C60560; RCRA waste number U213; UN 2056; diethylene oxide; dynasolve 150; QO tetrahydrofuran (THF); tetrahydrofurane;) is:

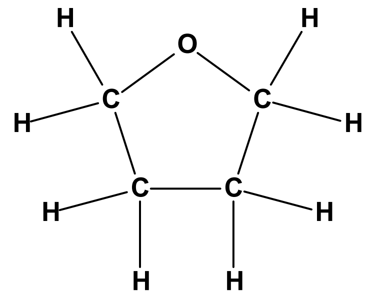

The normal boiling point is 339. ± 1. K as reported in the NIST Chemistry WebBook (Brown and Stein, Thermodynamics Research Center, Domalski and Hearing). Poling et al. report the boiling point as 339.12 K. The molecular mass is 72.1057 g/mol.

- **<u>Dihydrofuran (DHF)</u>**

The chemical structure of 2,3-dihydrofuran (4,5-dihydrofuran) is:

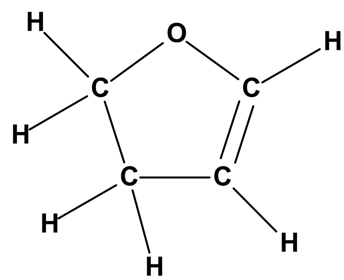

The normal boiling point is 327.7 and 328.15. ± 3. K as reported in the NIST Chemistry WebBook (Brown and Stein). The molecular mass is 70.0898 g/mol.

- **<u>Dimethylfuran (DMF)</u>**

The chemical structure of 2,5-dimethylfuran (2,5-dimethylfurane) is:

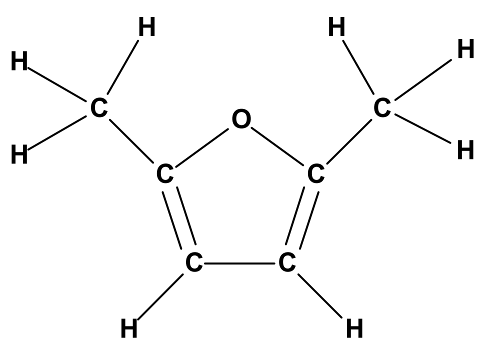

The normal boiling point is 367. ± 1. K as reported in the NIST Chemistry WebBook (Brown and Stein, Thermodynamics Research Center). The molecular mass is 96.1271 g/mol.

- **Methyltetrahydrofuran (MTHF)**

The chemical structure of tetrahydro-2-methylfuran (tetrahydrosylvan; 2-methyltetrahydrofuran; furan, 2-methyl-tetrahydro-; methyltetrahydrofuran; 2-methyloxolane; tetrahydrofuran, 2-methyl-;
2-methylfuranidine) is:

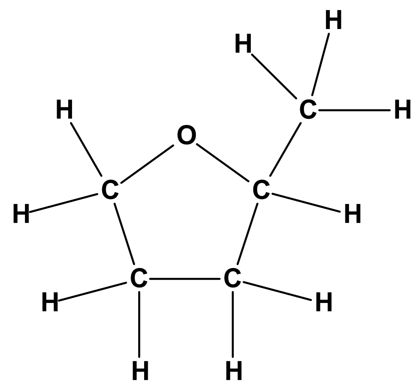

The normal boiling point is 352 ± 10 K as reported in the NIST Chemistry WebBook (Brown and Stein, Thermodynamics Research Center). Poling et al. report the boiling point as 353.37 K. The molecular mass is 86.1323 g/mol.

- **Methyldihydrofuran (MDHF)**

The chemical structure of 2,3-dihydro-5-methyl-furan (2-methyl-4,5-dihydrofuran; 2,3-dihydro-5-methylfuran; 4,5-dihydro-2-methylfuran; 5-methyl-2,3-dihydrofuran; 4,5-dihydrosylvan) is:

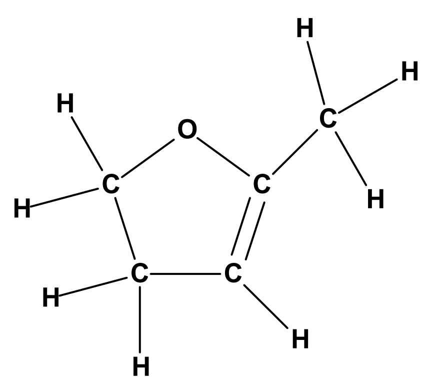

Values for the normal boiling point are 355.2 and 354.65 ± 1.5 K as reported in the NIST Chemistry WebBook (Brown and Stein). The molecular mass is 84.1164 g/mol.

- **Pyran**

The chemical structure of 4H-pyran is:

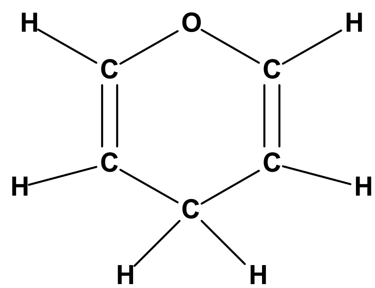

The normal boiling point is not reported in the NIST Chemistry WebBook. The molecular mass is 82.1005 g/mol.

- **Tetrahydropyran (THP)**

The chemical structure of tetrahydro-2H-pyran (tetrahydropyran; oxacyclohexane; oxane; pentamethylene oxide; THP) is:

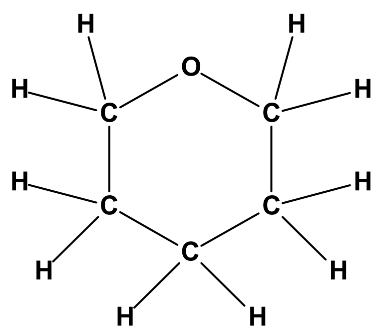

The normal boiling point is 361.0 ± 0.7 K as reported in the NIST Chemistry WebBook (Brown and Stein, Thermodynamics Research Center). The molecular mass is 86.1323 g/mol.

- **Dihydropyran (DHP)**

The chemical structure of 3,4-dihydro-2H-pyran (δ(sup2)-dihydropyran; 2,3-dihydro-4H-pyran; 2H-3,4-dihydropyran; 3,4-dihydro-2H-pyran; 3,4-dihydropyran; 5,6-dihydro-4H-pyran; 2,3-dihydropyran; 3,4-dihdro-2H-pyrane; 3,4-dihydro-2-pyran; δ2-dihydropyran; pyran, dihydro-) is:

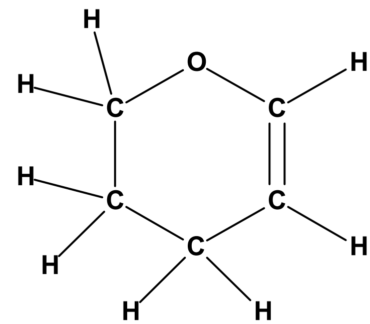

Values for the normal boiling point are 359.7, 359 ± 4 (Brown and Stein), 359 ± 2, and 358.85 ± 0.3 K (Thermodynamics Research Center) as reported in the NIST Chemistry WebBook. The molecular mass is 84.1164 g/mol.

- **Furfuryl Alcohol (FA)**

The chemical structure of 2-furanmethanol (furfuryl alcohol; α-furfuryl alcohol; α-furylcarbinol; furfuralcohol; furyl alcohol; furylcarbinol; 2-(hydroxymethyl)furan; 2-furancarbinol; 2-furanylmethanol; 2-furfuryl alcohol; 2-furylcarbinol; 2-furylmethanol; 5-hydroxymethylfuran; furfural alcohol; methanol, (2-furyl)-; NCI-C56224; 2-furfurylalkohol; UN 2874; 5-hydroxymethylfuranal; FA; QO furfuryl alcohol; 2-furanemethanol; 2-furane-methanol (furfurol); 2-furanmethanol (furfuryl alcohol); 2-hydroxymethylfurane; furan-2-methanol; furanmethanol; furfurol) is:

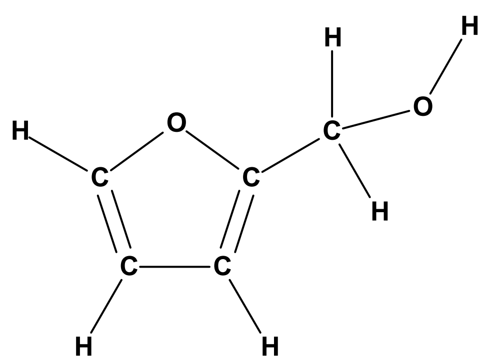

The normal boiling point is 430. ± 70. K as reported in the NIST Chemistry WebBook (Brown and Stein, Thermodynamics Research Center). The molecular mass is 98.0999 g/mol.

- **Methylhydroxymethylfuran (MHMF)**

The chemical structure of 5-methyl, 2-furanmethanol, ((5-Methyl-2-furyl)methanol; 5-methyl-2-furfuryl alcohol; (5-methylfurfur-2-yl)-methanol; 5-methylfurfuryl alcohol) is:

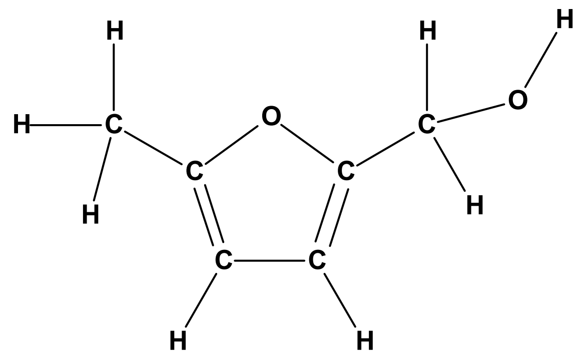

The normal boiling point is not reported in the NIST Chemistry WebBook. The molecular mass is 112.1265 g/mol.

- **Dihydroxymethylfuran (DHMF)**

The chemical structure of 2,5-dihydroxymethylfuran is:

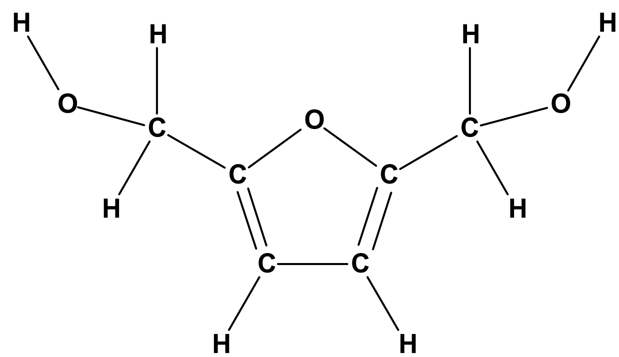

The normal boiling point is not reported in the NIST Chemistry WebBook. The molecular mass is 128.1259 g/mol.

2.1.2.2 Critical and normal properties of HMF. The normal boiling point of HMF is not reported in the NIST Chemistry WebBook. Román-Leshkov et al. report the value of 564 K (2007). The Marrero-Pardillo bond contribution method was used to estimate the normal boiling point of HMF and several other molecules of similar structure for which data are published (Marrero-Marejón and Pardillo-Fontdevila, 1999). The results are given in Table 2.2

Table 2.2 Normal Boiling Point Estimates and Comparison with Reported Values

Bond	**Contri-bution** χ_{T_b}	**Pair #**	**Bond Incidence** η_b							
			HMF	Furfural	Furan	MF	THF	DHF	DMF	MTHF
-CH[=][r]&-CH[=][r]	-0.2246	130		1	2	1		1		
=CH-[r]&=CH-[r]	0.2089	133	1	1	1	1			1	
=CH-[r]&-O-[r]	0.1000	135		1	2	1		1		
=C<[r]&-O-[r]	0.1104	143	2	1		1			2	
-CH[=][r]&>C[=][r]	-0.3586	131	2	1		1			2	
=C<[r]&-CHO	0.0919	152	1	1						
-CH2-&=C<[r]	0.1012	37	1							
-CH2-&-OH	-0.0786	42	1							
-CH2-[r]&-O-[r]	-0.0092	117					2	1		1
-CH2-[r]&-CH2-[r]	-0.0098	112					3	1		2
CH3-&=C<[r]	0.0987	10				1			2	
-CH2-[r]&=CH-[r]	0.0976	115						1		
CH3-&>CH-[r]	-0.0214	8								1
>CH-[r]&-O-[r]	-0.0218	125								1
-CH2-[r]&>CH-[r]	-0.0093	113								1
Predicted Value (K)			535.3	423.9	310.9	348.0	343.6	322.9	381.6	351.7
Reported Values (K)										
NIST				434.7	304.7	337.	339.	327.7 328.15	367.	352
PPOC					304.44	337.87	339.12			353.37
RPP				434.9	304.5	338.	338.			351.
RBLD			564	435		336			366	
Accepted Value (K)			564	434.7	304.7	337.	339.	327.7	367.	352
Absolute Error (K)			-28.7	-10.8	6.2	11.0	4.6	-4.8	14.6	-0.3
Percentage Error (%)			-5.1	-2.5	2.0	3.3	1.4	-1.5	4.0	-0.1

NIST--National Institute for Standards and Technology Chemistry WebBook (http://webbook.nist.gov/chemistry/) on July 1, 2009
PPOC--Poling, B. E, J. M. Prausnitz, and J. P. O'Connell, **The Properties of Gases and Liquids**, 5th Edition, McGraw-Hill, (2000)
RPP—Reid, R. C., J. M. Prausnitz, and B. E. Poling, **The Properties of Gases and Liquids**, 4th Edition, McGraw-Hill, (1987)
RBLD-- Roman-Leshkov, Y, C. J. Barrett, Z. Y. Liu, and J. A. Dumesic, **Nature**, **447**, (June 21, 2007) p. 982

Table 2.2 Normal Boiling Point Estimates and Comparison with Reported Values (cont.)

Bond	**Contri-bution** χ_{T_b}	**Pair #**	**Bond Incidence** η_b						
			MDHF	Pyran	THP	DHP	FA	MHMF	DHMF
-CH[=][r]&-CH[=][r]	-0.2246	130		2		1	1		
=CH-[r]&=CH-[r]	0.2089	133					1	1	1
=CH-[r]&-O-[r]	0.1000	135		2		1	1		
=C<[r]&-O-[r]	0.1104	143	1				1	2	2
-CH[=][r]&>C[=][r]	-0.3586	131	1				1	2	2
=C<[r]&-CHO	0.0919	152							
-CH2-&=C<[r]	0.1012	37					1	1	2
-CH2-&-OH	-0.0786	42					1	1	2
-CH2-[r]&-O-[r]	-0.0092	117	1		2	1			
-CH2-[r]&-CH2-[r]	-0.0098	112	1		4	2			
CH3-&=C<[r]	0.0987	10	1					1	
-CH2-[r]&=CH-[r]	0.0976	115	1	2		1			
CH3-&>CH-[r]	-0.0214	8							
>CH-[r]&-O-[r]	-0.0218	125							
-CH2-[r]&>CH-[r]	-0.0093	113							
Predicted Value (K)			359.0	325.1	364.0	344.7	443.8	471.3	552.7
Reported Values (K)									
NIST			355.2 354.65		361.0	359.7 359 359 358.85	430		
PPOC									
RPP					361.	359.			
RBLD							435	452	548
Accepted Value (K)			355.2		361.0	359.7	435	452	548
Absolute Error (K)			3.8		3.0	-15.0	8.8	19.3	4.7
Percentage Error (%)			1.1		0.8	-4.2	2.0	4.3	0.9

NIST--National Institute for Standards and Technology Chemistry WebBook (http://webbook.nist.gov/chemistry/) on July 1, 2009
PPOC--Poling, B. E, J. M. Prausnitz, and J. P. O'Connell, **The Properties of Gases and Liquids**, 5th Edition, McGraw-Hill, (2000)
RPP—Reid, R. C., J. M. Prausnitz, and B. E. Poling, **The Properties of Gases and Liquids**, 4th Edition, McGraw-Hill, (1987)
RBLD-- Roman-Leshkov, Y, C. J. Barrett, Z. Y. Liu, and J. A. Dumesic, **Nature**, **447**, (June 21, 2007) p. 982

The bond contribution values are those reported in Poling et al. (2000). The equation that relates the bond contributions to the normal boiling point is:

$$T_b = 156.00 + M^{-0.404} \sum \eta_b \chi_{T_b} \tag{1}$$

- T_b Estimate for the normal boiling point (K)
- M Molecular mass (g/mol)
- η_b Bond incidence
- χ_{T_b} Bond contribution for the normal boiling point

The predicted value for the normal boiling point of HMF is 535.3 K. The error between the predicted boiling point and the reported value is -28.7 K or -5.1%. Unfortunately, these errors are larger than those of the other 13 compounds of similar structure that were examined. HMF has the highest reported boiling point of the compounds in the analysis. The database used to determine the bond contributions would be unlikely to contain higher values for molecules containing furan bonds. However, the errors for the 13 compounds with reported data varied from -2.5% to +4.3% with no discernible pattern and an average absolute percentage error of 2.2%. The errors for the eight compounds that share at least one of the six bonds in HMF covered the full range from -2.5% to +4.3 with an average absolute percentage error of 2.5%. Poling et al. report an average absolute percentage error of 2.0% for 347 compounds using the Marrero-Pardillo method. Of the 347 compounds, only 29 had absolute percentage errors greater than 5% and only 10 were greater than 10%. The large error (-5.1%) between the predicted and reported values for the normal boiling point of HMF compared to the average error (±1.0%) for the Marrero-Padillo method reduces the confidence that other properties will be predicted within the average errors for the method. The reported value (564 K) was used.

The critical properties of HMF are not reported in the NIST Chemistry WebBook. The equations that relate the bond contributions to the critical properties are:

$$T_c = \frac{T_b}{0.5851 - 0.9286\sum \eta_b \chi_{T_c} - \left(\sum \eta_b \chi_{T_c}\right)^2} \tag{2}$$

$$P_c = \left[0.1285 - 0.0059 N_a - \sum \eta_b \chi_{P_c}\right]^{-2} \tag{3}$$

$$V_c = 25.1 + \sum \eta_b \chi_{V_c} \tag{4}$$

- T_c Estimate for the critical temperature (K)
- χ_{T_c} Bond contribution for the critical temperature
- N_a Number of atoms in the molecule
- χ_{P_c} Bond contribution for the critical pressure
- χ_{V_c} Bond contribution for the critical volume

The accepted value (Table 2.2) for the normal boiling point was used to estimate the critical temperature (except for pyran) not the value predicted by the Marrero-Pardillo method. The predicted values for the critical properties of HMF are 787.9 K, 56.4 bar, and 229.9 cm^3/mole. These values give a critical compressibility factor for HMF of 0.1998. A comparison with reported values for compounds with similar structure is given in Table 2.3. The seven compounds with reported values for the critical temperature had percentage errors that ranged from -0.7% to +1.0% with an average absolute percentage error of 0.4%. The three compounds that share bonds with HMF had a range of -0.5% to +0.3% and an average of 0.3%. Poling et al. report an average absolute percentage error of 0.9% for 343 compounds using the Marrero-Pardillo method using reported values for the normal boiling point. Of the 343 compounds, only 7 had absolute percentage errors greater than 5% and only one was greater than 10%. The seven compounds with reported values for the critical pressure had percentage errors that ranged from -4.3% to +12.6% with an average absolute percentage error of 7.8%. The three compounds that share bonds with HMF had a range of +7.9% to +12.6% and an average of 10.2%. Poling et al. report an average absolute percentage error of 5.3% for 338 compounds using the Marrero-Pardillo method. Of the 338 compounds, 110 had absolute percentage errors greater than 5% of which 47 were greater than 10%. The six compounds with reported values for the critical volume had percentage errors that ranged from -0.5% to +3.9% with an average absolute percentage error of 1.2%. The two compounds that share bonds with HMF had percentage errors of -0.5% and 0% and an absolute average of 0.3%. Poling et al. report an average absolute percentage error of 3.2% for 296 compounds using the Marrero-Pardillo method. Of the 296 compounds, 55 had absolute percentage errors greater than 5% of which 18 were greater than 10%.

Table 2.3 Critical Property Estimates and Comparison with Reported Values

	Chemical Species														
CRITICAL TEMPERATURE	HMF	Furfural	Furan	MF	THF	DHF	DMF	MTHF	MDHF	Pyran	THP	DHP	FA	MHMF	DHMF
Predicted Value (K)	787.9	672.1	490.7	525.4	540.5	523.7	555.5	538.2	549.9	514.1	568.3	567.5	624.7	635.0	729.3
Reported Values (K)															
NIST		670.	490.2 490.2 487.	528.	540.2 540.1 541.			537.			572.2	561.7			
PPOC			490.15	527.85	540.20			537.00							
RPP		670.	490.2	527.				537.			572.2	561.7			
Accepted Value (K)		670.	490.2	528.	540.2			537.			572.2	561.7			
Absolute Error (K)		2.1	0.5	-2.6	0.3			1.2			-3.9	4.2			
Percentage Error (%)		0.3	0.1	-0.5	0.1			0.2			-0.7	1.0			
CRITICAL PRESSURE	HMF	Furfural	Furan	MF	THF	DHF	DMF	MTHF	MDHF	Pyran	THP	DHP	FA	MHMF	DHMF
Predicted Value (bar)	56.4	59.4	59.9	52.0	49.7	53.4	45.5	40.6	46.7	54.0	46.7	50.2	56.8	49.4	53.9
Reported Values (bar)															
NIST		55.1	53.2	47.2	51.9			37.5763			47.7	45.6			
PPOC			55.00	47.20	51.90			37.60							
RPP		58.9	55.0	47.2				37.6			47.7	45.6			
Accepted Value (bar)		55.1	53.2	47.2	51.9			37.6			47.7	45.6			
Absolute Error (bar)		4.3	6.7	4.8	-2.2			3.0			-1.0	4.6			
Percentage Error (%)		7.9	12.6	10.1	-4.3			8.0			-2.0	10.0			
CRITICAL VOLUME	HMF	Furfural	Furan	MF	THF	DHF	DMF	MTHF	MDHF	Pyran	THP	DHP	FA	MHMF	DHMF
Predicted Value (cm^3/mole)	229.9	175.3	218.0	247.0	225.1	220.8	276.0	273.7	249.8	263.7	272.3	268.0	272.6	301.6	327.2
Reported Values (cm^3/mole)															
NIST			219.	247.	225.			267.			262.				
PPOC			218.00	246.40	224.00			267.00							
RPP			218.	247.				267.			263.	268.			
Accepted Value (cm^3/mole)			219.	247.	225.			267.			262.	268.			
Absolute Error (cm^3/mole)			-1.0	0	0.1			6.7			10.3	0			
Percentage Error (%)			-0.5	0	0.0			2.5			3.9	0			

NIST--National Institute for Standards and Technology Chemistry WebBook (http://webbook.nist.gov/chemistry/) on July 1, 2009
PPOC--Poling, B. E, J. M. Prausnitz, and J. P. O'Connell, **The Properties of Gases and Liquids**, 5th Edition, McGraw-Hill, (2000)
RPP—Reid, R. C., J. M. Prausnitz, and B. E. Poling, **The Properties of Gases and Liquids**, 4th Edition, McGraw-Hill, (1987)

2.1.2.3 Vapor pressure of HMF. Vapor pressure regressed from the Clausius-Clapeyron equation for the vapor pressure of HMF using the normal boiling and critical points is (Koretsky, 2004):

$$P = e^{-7977/T + 25.67} \tag{5}$$

- P Vapor pressure in pascal
- T Temperature in K

2.1.2.4 Liquid molar volume of HMF. The Rackett equation was used to estimate liquid molar volume using critical temperature, critical volume and critical compressibility factor (1970):

$$Z_c = \frac{P_c V_c}{T_c R} \tag{6}$$

$$V_f = \frac{RT_c}{P_c} Z_c^{\,1+(1-T_r)^{2/7}} \tag{7}$$

- Z_c Critical compressibility factor
- V_c Critical volume
- V_f Liquid molar volume
- T_r Reduced temperature
- R Ideal gas constant

$Z_c = 0.198$

$V_f = 0.05589$ L/mol

2.1.2.5 Ideal gas heat of formation and heat capacity of HMF. Enthalpy of formation for HMF is not reported in the NIST Chemistry Webook. The Benson group method was used to estimate the ideal gas heat of formation and heat capacity at temperatures from 298 to 1000 K (Poling et al., 2000).

The Benson Group Method

$$\Delta H_f{}^\circ(298.15K) = \sum_k N_k(\Delta H_{fk}{}^\circ) \tag{8}$$

$$C_p{}^\circ(T) = \sum_k N_k C_{pk}{}^\circ(T) \tag{9}$$

- $\Delta H_f{}^\circ$ Enthalpy of formation at 298 K
- $C_p{}^\circ(T)$ Heat capacity at temperature T
- N_k Incidence number for group k
- $H_{fk}{}^\circ$ Group contribution for enthalpy of formation
- $C_{pk}{}^\circ(T)$ Group contribution for heat capacity at temperature T

Table 2.4 contains the incidence numbers, the group contribution values, and the property values. The group contribution values are those reported in Poling et al. (2000).

The Benson group method produces estimates for heat capacities over a range of temperatures. These were further regressed to fit ASPEN’s CPIG equation.

$$C_p = -2.284\times10^{-4}T^2 + 0.5259T - 5.2344 \tag{10}$$

- C_p heat capacity in J/molK

Table 2.4 Benson Group Contribution Method

Group	N_k	$\Delta H°_f$ 298K kJ/mol	$C°_p$ 298K J/molK	$C°_p$ 400K J/molK	$C°_p$ 500K J/molK	$C°_p$ 600K J/molK	$C°_p$ 800K J/molK	$C°_p$ 1000K J/molK
OH—(C)	1	-158.56	18.12	18.63	20.18	21.89	25.2	27.67
CH2—(=C,O)	1	-27.21	19.51	29.18	36.21	41.36	48.3	53.29
=C—(C,O)	1	43.11	17.16	19.3	20.89	22.02	24.28	25.45
=CH—(=C)	2	28.38	18.67	24.24	28.25	31.06	34.95	37.63
=C—(CO,O)	1	31.39	22.94	29.22	31.02	31.98	33.53	34.32
O—(2=C)	1	-138.13	14.02	16.32	17.58	18.84	21.35	22.6
(CO)H—(=C)	1	-121.81	24.32	30.22	39.77	48.77	63.12	74.68
Furan ring	1	37.25	-20.51	-18	-15.07	-12.56	-10.88	-10.05
Property Value		-277.2	132.9	173.35	207.08	234.42	274.8	303.22

2.1.3. UNIFAC Parameters. The UNIFAC method was used to estimate activity coefficients (Seader and Henley, 2006). Values for group volume, surface area, and energy interaction parameters are required by the UNIFAC method. Furfural, a common solvent, has its own group and main group. As such, values for group volume and surface area for this group are available. However, group values for furfural with a hydrogen atom removed from the ring is required for the constituent group in HMF.

HMF can be considered to be a combination of the following structural groups:

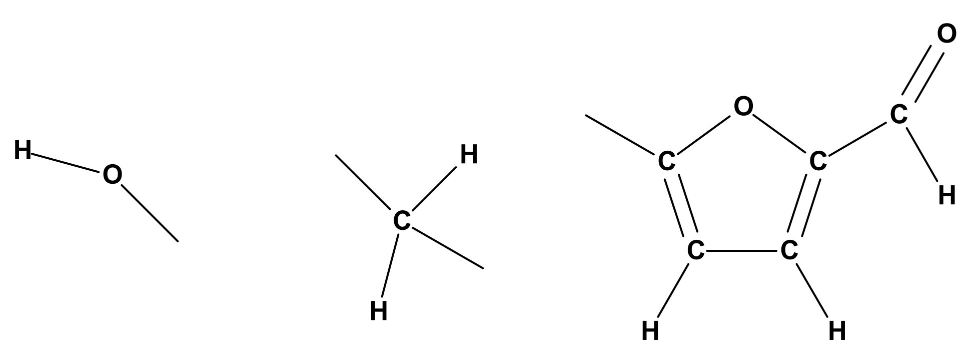

The UNIFAC parameter values are tabulated for the –OH and –CH_2- groups. There are tabulated UNIFAC parameter values for furfural (C_4H_3O-CHO), but not for the -C_4H_2O-CHO group.

The -C_4H_2O-CHO group is the furfural group with a hydrogen atom removed from the ring. There are tabulated values for other groups that differ by a hydrogen atom removed from the ring. Table 2.5 shows the UNIFAC parameter values and main group assignments for hydrogen atom removal from carbon atoms in aromatic rings, pyridine rings, and thiophene rings.

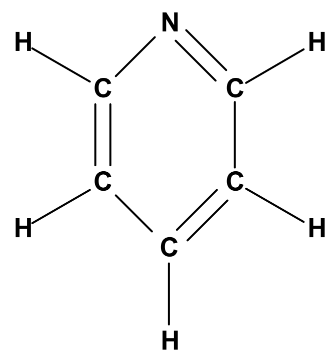

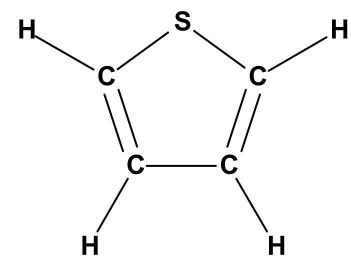

Table 2.5 UNIFAC Parameter Values for Ring Groups

Ring	Group	Main Group Assignment	Group Volume R	Hydrogen Atom Volume Contribution ΔR	Group Surface Area Q	Hydrogen Atom Surface Area Contribution ΔQ
Aromatic	ACH	3	0.5313	0.1663	0.400	0.280
	-AC	3	0.3652		0.120	
Pyridine	C_5H_5N	18	2.9993	0.1661	2.113	0.280
	- C_5H_4N	18	2.8332	0.1662	1.833	0.280
	> C_5H_3N	18	2.6670		1.553	
Thiophene	C_4H_4S	50	2.8569	0.1661	2.140	0.280
	-C_4H_3S	50	2.6908	0.1661	1.860	0.280
	>C_4H_2S	50	2.5247		1.580	
Furfural	C_4H_3O-CHO	30	3.1680	0.1662	2.481	0.280
	-C_4H_2O-CHO	30	3.0018		2.201	

The removal of a hydrogen atom from various rings (aromatic, pyridine, thiophene) results in a uniform reduction in both group volume (0.1662 ± 0.0001) and surface area (0.280) for primary or secondary substitutions (Table 2.5). Further, the groups with common ring types are assigned to the same main group. These data provide UNIFAC parameter estimates for the $-C_4H_2O-CHO$ group (Table 2.5) derived from the values for furfural and indicate that the group would be in the same main group as furfural and, therefore, have the same energy interaction parameters.

Group energy interaction parameters for furfural-water were regressed from in **Liquid-Liquid Equilibrium Data Collection (J.M. Sørensen, W. Arlt.)** specifically for the temperature range of 15 to 30 °C.

Other energy interaction parameters were taken from ASPEN's LLE group energy interaction parameter set as presented in ASPEN's Appendix Table 3.15. The values used in the simulation can be found in Table 2.6

Table 2.6 Group Energy Interaction Parameters (K)

ASPEN Group ID	2450 & 4001	1300	1010	1200
Group	Furfural	Water	>CH2	OH-P
Furfural	0	165.562	-25.31	521.6
Water	111.266	0	300	-229.1
>CH2	354.6	1318	0	986.5
OH (primary)	-120.5	353.5	156.4	0

These values predict a Type 2 liquid-liquid equilibrium as show in Figure 2.1.

Aspen Distillation Synthesis Distillation Analysis - Ternary Map

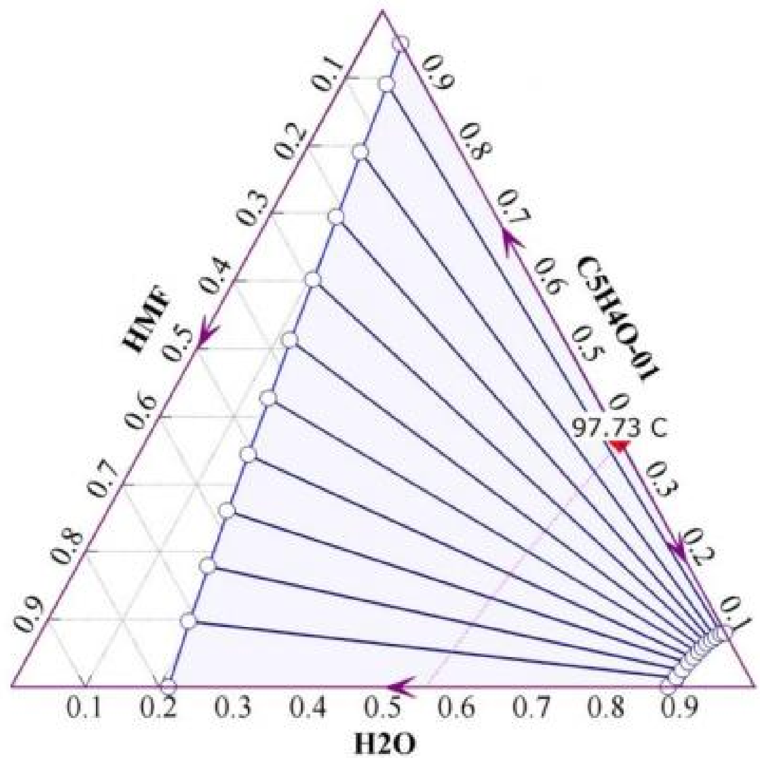

Ternary Map computed at the following conditions :

Pressure: 101325 N/SQM

Envelope Type: Liquid-Liquid at 20 C

VLE/VLLE Model: UNIF-LL

LLE Model:UNIF-LL

Vaild Phases: Vapor-Liquid-Liquid

Basis: Mass fraction

Figure 2.1 Furfural-HMF-Water Ternary Diagram

2.2. PROPERTIES OF SOLIDS

The parameter values for correlations of the properties of cellulose and xylan are listed in Table 2.7 (Wooley and Putsche, 1996). ASPEN's solid property formulas for the methods used are given following Table 2.7

Table 2.7 Solids Property Data

Property	Aspen Property	Units	Xylan	Cellulose
Molecular Weight	MW		132.117	162.1436
Solid Heat of Formation	DHFORM	kJ/Kmole	-762416	-976362
Solid Molar Volume	VSPOLY/1	cum/Kmole	0.0864	0.1060
	VSPOLY/2			
	VSPOLY/3			
	VSPOLY/4			
	VSPOLY/5			
	VSPOLY/6		298.15	298.15
	VSPOLY/7		1000	1000
Solids Heat Capacity	CPSPO1/1	J/Kmol K	-9529.9	-11704
	CPSPO1/2		547.25	672.07
	CPSPO1/3			
	CPSPO1/4			
	CPSPO1/5			
	CPSPO1/6			
	CPSPO1/7		298.15	298.15
	CPSPO1/8		1000	1000

Solid Volume Polynomial VSPOLY/1….

$$V^*(T) = C_1 + C_2T + C_3T^2 + C_4T^3 + C_5T^4 \text{ for } C_6 \leq T \leq C_7 \qquad (11)$$

Solid Heat Capacity CPSP01/1….8

$C_p(T) = C_1 + C_2T + C_3T^2 + C_4/T + C_5/T^2\ C_6/SQRT(T)$ for $C_7 \leq T \leq C_8$ (12)

2.3. REACTION KINETICS

Currently available data for reaction rate consist of that presented in the patent filing (Petrus and Voss, 2005). The results of five experiments are reported in which biomass feedstock, solvent, acid and acid concentration, temperature and time vary in the different experiments. This data set only records the solid residue left after the reaction, making no distinction between pentosans, hexosans or other organic compounds. To approximate reaction rate the data given in the patent is regressed based on a first order reaction rate with mass basis. This assumes that the reaction rate is independent of biomass feedstock, solvent, acid, acid concentration and that the reaction rate is first order. Data from the experiments is presented in Table 2.8 with the linear regression ($R^2 = 0.8397$) for the first order reaction plotted Figure 2.2. Finally the reaction rate as a function of temperature is presented in Figure 2.3.

The resulting rate law

$$E_a/R = -13721\ K \tag{13}$$

$$\ln k_\infty = 25.901 \tag{14}$$

$$\frac{dm}{dt} = mk \tag{15}$$

$$k = k_\infty e^{-E_a/RT} \tag{16}$$

- m fraction of the original mass
- k given in inverse minutes

Table 2.8 Reaction Rate Data for Solvent Liquefaction

Biomass	Solvent	Acid	Temperature [C]	Time [min]	% residue	ln(k)	1/T [K^{-1}]
Birch sawdust	gammaVL	H_3PO_4	200	60	0.16	-3.488	0.002114
Birch sawdust	gammaVL	H_3PO_4	180	240	0.1	-4.646	0.002208
Birch sawdust	gammaVL	H_3PO_4	184	180	0.18	-4.654	0.002188
Birch sawdust	gammaVL	H_3PO_4	230	16	0.03	-1.518	0.001988
Bagasse	Levulinic acid	H_2SO_4	190	60	0.04	-2.925	0.002160

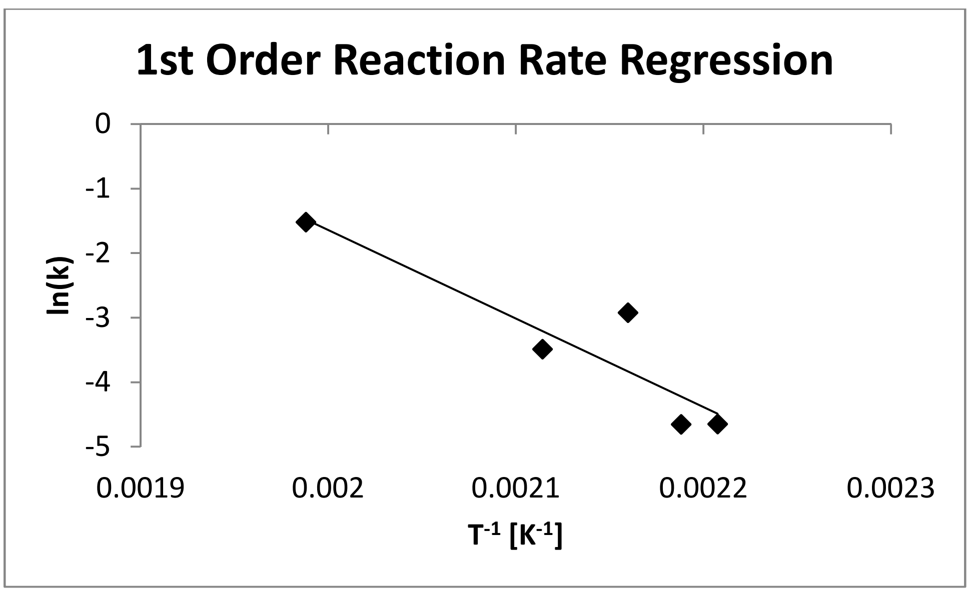

Figure 2.2 Reaction Rate Regression

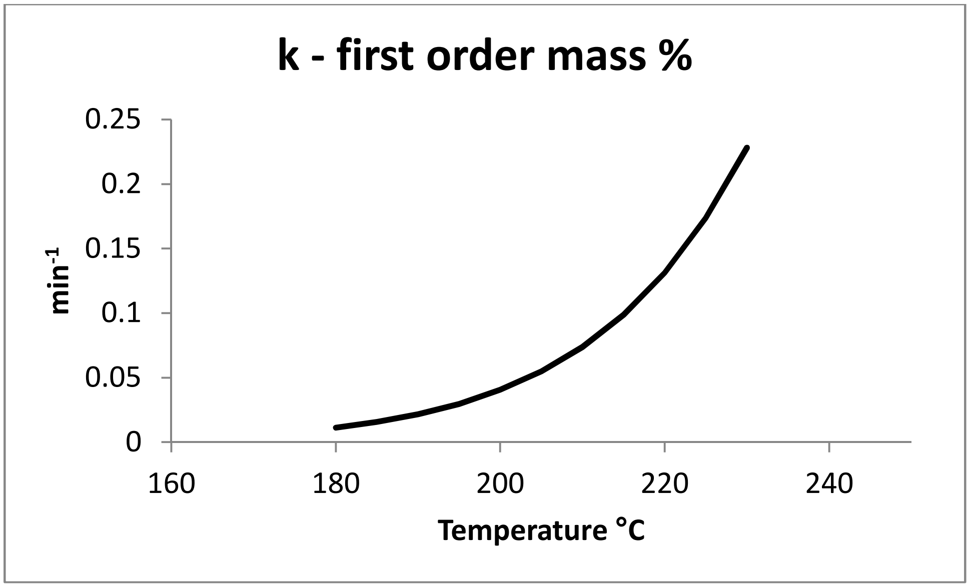

Figure 2.3 Regressed Reaction Rate as a Function of Temperature

3. SIMULATION

3.1. PROCESS DESCRIPTION

3.1.1. Process. The process is continuous. As seen in Figure 3.1 the feed (stream #1) is sent to the reactor (vessel B1) where it is heated to the reactor temperature. The reactor product (stream #2) is cooled and sent to the decanter (vessel B2) where the two liquid phases, organic (stream #4) and aqueous (stream #5) are separated. All unreacted solids are part of the aqueous phase. The vapor product (stream #3) is unused.

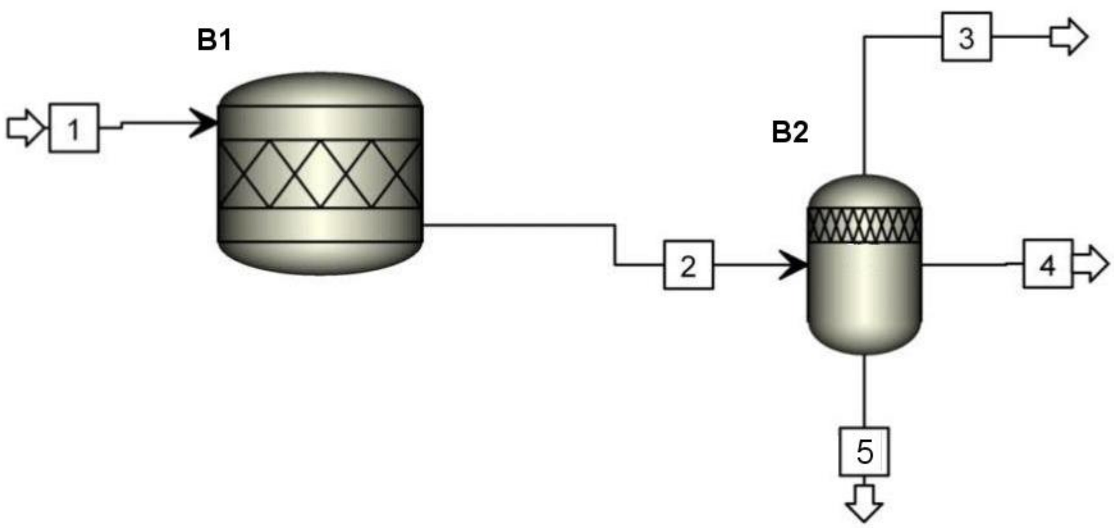

Figure 3.1 Simulation Process Flow Diagram

3.1.2. Reactor. In the process simulation, the reactor provides heating and a vessel for the reaction. Due to limitations in ASPEN a "Stoichiometric" reactor is used. Temperature, conversion and vapor fraction of the reactor are specified.

$$\underset{\text{Xylan}}{nC_5H_8O_4} + nH_2O \longrightarrow \underset{\text{Xylose}}{nC_5H_{10}O_5} \longrightarrow \underset{\text{Furfural}}{nC_5H_4O_2} + 3n\,H_2O$$

$$\underset{\text{Cellulose}}{nC_6H_{10}O_5} + nH_2O \longrightarrow \underset{\text{Glucose}}{nC_6H_{12}O_6} \longrightarrow \underset{\text{HMF}}{nC_6H_6O_3} + 3n\,H_2O$$

Only the complete reactions will be considered such that the reactions simulated are simplified.

$$nC_5H_8O_4 + nH_2O \longrightarrow nC_5H_4O_2 + 3n\,H_2O$$

$$nC_6H_{10}O_5 + nH_2O \longrightarrow nC_6H_6O_3 + 3n\,H_2O$$

3.1.3. Phase Separator. The phase separator or decanter separates the less dense organic liquid phase from the aqueous phase and solids. Temperature is specified to be 20 °C, and vapor fraction to be 0. The UNIFAC group interaction parameters for furfural and water were regressed using data from a temperature range of 15-30° C, an appropriate choice for the simulation.

3.2. FEEDSTOCK

The simulation feedstock was intended to approximate corn stover. The moisture content of biomass is taken to be 55% (Sokhansanj et al., 2002).

Cellulose and xylan were taken to be a representative species for all hexosans and pentosans respectively. The split between pentosans and hexosans of corn stover was taken to be 27.5% pentosans and 72.5% hexosans (Kamm et al., 2006).

Runs were done with feedstock composition of pure xylan, pure cellulose and the 27.5%-72.5% mixture. The simulated feedstock contained only xylan, cellulose and water. No lignin was included in any of the simulated feedstocks. Simulation feedstock was set at a temperature of 25 °C and atmospheric pressure.

4. SIMULATION RESULTS

Based on the predicted physical property data, the heat of reaction for the formation of both furfural and HMF varies with temperature. Both reactions have very small heats of reaction that become increasingly endothermic as the temperature is increased (Figure 4.1).

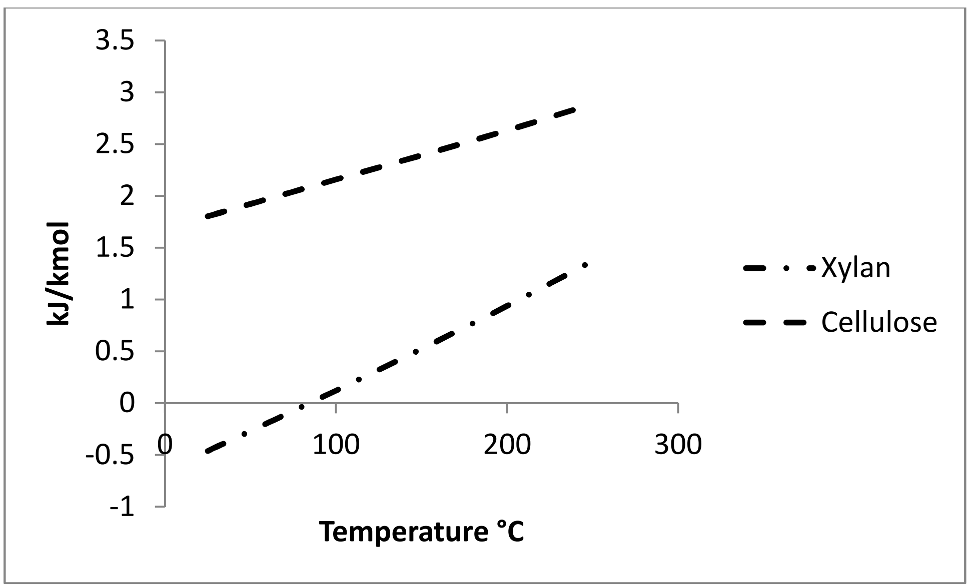

Figure 4.1 Heat of Reaction as a Function of Temperature

The simulation was run for feedstocks at 55% moisture content, containing pure xylan, pure cellulose and the mixture approximating corn stover. Runs were conducted at three temperatures over the range of data provided in the patent.

Of great interest is how much chemical energy is available in the product less the amount of energy required by the process, relative to the total chemical energy input into the process. The laws of thermodynamics will prevent this value from being greater than one. Zero values reflect the product only has as much energy as was required by the process. Values less than zero are possible. These occur when more energy is required by the process than is available in the feed.

Figure 4.2 shows that the fractional energy return (equation 17) of the process is positive for a wide range of conversions and that the extent of reaction and not feedstock composition is the primary determining factor of fractional energy return. The complete table of simulation run results is available in Appendix B. Two of the sample data points for cellulose did not contain enough HMF to result in a phase split. As a result all of the HMF in these simulation runs was recovered in the organic phase resulting in higher fractional energy recovery. One point lies off of the line at a conversion of 0.28. The other is at a conversion of 0.017 and has a slightly higher fractional energy recovery than the all xylan feed simulation at the same conversion.

$$q = \frac{\begin{matrix} enthalpy\ of\ combustion\ of\ furfural \\ and\ hmf\ in\ organic\ phase \end{matrix} - process\ energy\ requirements}{enthalpy\ of\ combustion\ of\ feed} \tag{17}$$

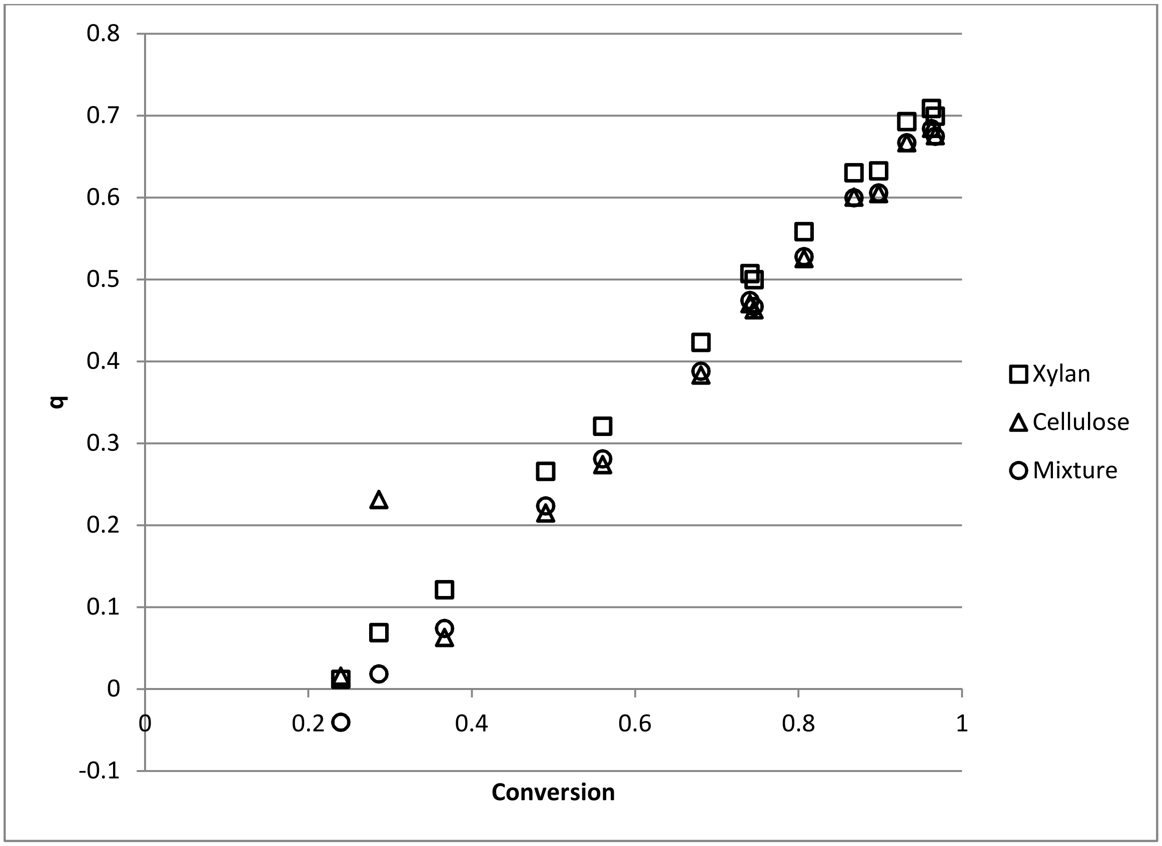

Figure 4.2 Product Energy Recovery Ratio as a Function of Conversion

Figure 4.3 shows the ratio of enthalpy of combustion of the organic product to process energy requirement which varied with conversion, temperature and feed composition. Product to process energy ratios decreased with increasing temperatures and, with the exceptions of the two previously noted points where a phase split did not occur, increased with conversion and were higher for xylan than cellulose at the same conversion and temperature. The range of ratios increased with conversion and varied from 7 to 11.5 for high conversion.

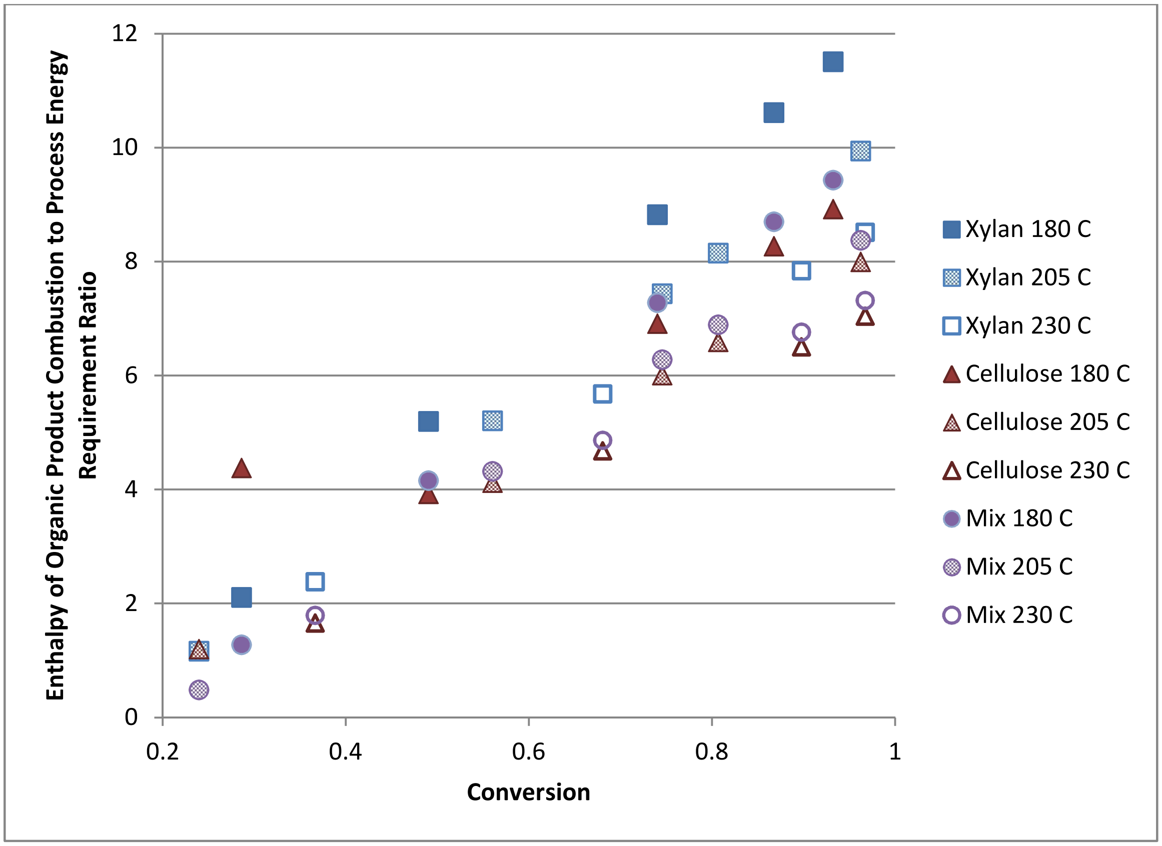

Figure 4.3 Product Energy to Process Energy as a Function of Conversion

5. DISCUSSION

Many physical properties were estimated as detailed in Section 2. If more accurate estimates or experimental data become available, the simulation may be updated to reflect this. This also applies to the liquefaction reaction where limited data resulted in many assumptions being made in estimating a reaction rate. Additional investigation should seek to detail the effects of solvent and acid on the reaction rate as well as identifying if lignin is being reacted in addition to cellulose and hemicellulose.

As described in Section 3.1.1 the simulation's only energy input requirement is heating the feed. While a range of reactor temperatures were simulated, the increased heating requirement for higher temperatures was of little significance compared to conversion in the final fractional energy recovery. Given the faster reaction rate at higher temperatures, operation at these higher temperatures is likely to be more economical. Future simulations could seek to detail additional energy requirements for cooling, pumping, mixing, etc. The simulation does not include an economizer, a heat exchanger that would use the reactor product to heat the feed while being cooled. The economizer would lower the feed heating requirement, improving the processes energy recovery ratio.

Figure 2.1, the ternary map, shows that more HMF than furfural will be in the aqueous phase. Despite this the simulated biomass feed's ratio of cellulose to xylan had a limited effect on the process energy ratio. Only energy density and liquid-liquid equilibrium could have caused any such difference in the simulation since the reaction rate was assumed to be the same on a mass basis for both species. Further studies could seek to analyze liquefaction of both cellulose and xylan separately.

The moisture content of the feed is expected to play an important role in the process energy ratio but was not studied in this thesis. The simulation could be used to further investigate the effects of biomass moisture content on process energy recovery ratio. Additional moisture in the feed will result in increased heating requirements and shift the liquid-liquid equilibrium.

The liquefaction process simulation indicates that much of the chemical energy in the biomass feedstock can be recovered as an organic rich phase. Further, high recovery ratios are achieved at short residence times required for field liquefaction. For field liquefaction, energy expended to grow and harvest grain and biomass coproducts can be charged to the grain (as must be done when the biomass is returned to the field). The energy in an organic liquid coproduct is achieved at the energy cost of the liquefaction process. Simulation of the simplified liquefaction process indicated an energy recovery ratio of 2/3 could be obtained. Some of the loss is due to unreacted biomass and some to process energy requirements. Feed composition, cellulose or xylan did not result in major differences in this ratio.

The ratio of enthalpy of combustion in the product to process energy requirement varied with conversion, temperature and feed composition as seen in Figure 4.3. There is a clear tradeoff between reactor temperature and process energy requirement. The higher temperatures allows for lower residence times and thus a smaller reactor for the same conversion. The lowest temperature (180 C), highest conversion and the mixed feedstock had a product to process energy ratio of over 9:1. This is much greater than the 5:4 ratio for grain ethanol reported by Graboski (2002), where the energy expended growing the grain must be charged to the ethanol, and larger than the 2.61:1 value quoted for enzymatic ethanol (Lorenz 1995).

With an energy recovery ratio above those for ethanol processes the furfural-HMF liquefaction clearly deserves further study. While not as high as petroleum derived products energy recovery ratio of 1:14 the furfural-HMF process competes on its renewable benefits and not energy efficiency alone.

Further development of the process simulation will bring it closer to modeling all of the steps presented in Figure 1.3, including neutralizing acid used, solvent recovery, and treatment of the aqueous phase and unreacted biomass.

APPENDIX A.

ASPEN SIMULATION FILES

Relevant ASPEN documents are included in an attached folder.

Simulation PFD.PNG Simulation Process Flow Diagram Image
Phase Diagrams and PFD.pdf
final simulation.inp Input Summary
final simulation.rep Sample Run
final simulation.apmbd
final simulation.apw
final simulation.bkp
final simulation.def
final simulation.dxf
final simulation.sum
reactor decater.bkp
aspen simulation runs.xlsx Spreadsheet and Charts of Simulation Results

APPENDIX B.

SIMULATION RESULTS

Run	Time	Temperature	Conversion
	Minutes	C	
1	30	180	0.286150764
2	60	180	0.490419268
3	120	180	0.740327477
4	180	180	0.867675886
5	240	180	0.932570181
6	5	205	0.239591703
7	15	205	0.560316122
8	25	205	0.745765646
9	30	205	0.806678087
10	60	205	0.962626638
11	2	230	0.366387184
12	5	230	0.680434503
13	10	230	0.897877893
14	15	230	0.967365298

Reaction rate is assumed to be first order mass basis. A range of temperatures and reaction times were used to calculate conversion for the simulation runs.

Xylan 12.38 kg/hr, Cellulose 32.625 kg/hr, Water 55 kg/hr, 25 C

										Enthalpy of Combustion		
		Organic Phase			Aqueous Phase					In Organic Phase		
Run	Heat Duty	Water	Furfural	HMF	Water	Furfural	HMF	Xylan	Cellulose	Furfural	HMF	Q
	Cal/sec	Kg/hr	Kg/hr	Kg/hr	Kg/hr	Kg/hr	Kg/hr	Kg/hr	Kg/hr	kJ/hr	kJ/hr	
1	3484	0.586	0.704	2.129	57.455	1.872	5.132	8.837	23.289	-17171.25462	-49768.10568	0.018414702
2	3692	2.012	2.483	7.294	58.199	1.932	5.15	6.309	16.625	-60562.81992	-170506.6054	0.223415514
3	3937	3.746	4.685	13.577	59.12	1.98	5.209	3.215	8.472	-114271.7726	-317379.789	0.474121847
4	4060	4.611	5.807	16.703	59.587	2.006	5.237	4.416	1.628	-141638.4596	-390454.0484	0.599656267
5	4126	5.081	6.386	18.403	59.829	2.011	5.26	0.835	2.2	-155760.8409	-430193.7289	0.666974078
6	4068	0.259	0.307	0.941	57.287	1.85	8.139	9.414	24.808	-7488.03291	-21997.08194	-0.040477224
7	4414	2.496	3.097	9.052	58.458	1.947	5.166	5.443	14.345	-75538.88574	-211602.1102	0.280965146
8	4609	3.784	4.733	13.713	59.14	1.981	5.21	3.147	8.294	-115442.5399	-320558.9634	0.466772255
9	4673	4.207	5.272	15.243	59.365	1.991	5.226	2.393	6.307	-128589.2818	-356324.6758	0.52782599
10	4836	5.289	6.651	19.157	59.94	2.016	5.269	0.463	1.219	-162224.4524	-447819.446	0.684030231
11	4879	1.148	1.399	4.164	57.745	1.9	5.133	7.844	20.672	-34122.99036	-97338.84079	0.073817394
12	5237	3.33	4.156	12.072	58.9	1.97	5.194	3.956	10.426	-101368.9406	-282198.4837	0.38796232
13	5480	4.841	6.079	17.533	59.7	2.006	5.25	1.264	3.332	-148272.808	-409856.363	0.605574728
14	5557	5.322	6.693	19.276	59.958	2.016	5.271	0.404	1.065	-163248.8738	-450601.2236	0.674799166

Xylan 45 kg/hr, Water 55 kg/hr, 25 C

		Organic Phase		Aqueous Phase			Enthalpy of Combustion in Organic Phase	
Run	Heat Duty	Water	Furfural	Water	Furfural	Xylan	Furfural	Q
	Cal/sec	Kg/hr	Kg/hr	Kg/hr	Kg/hr	Kg/hr	kJ/hr	
1	3297	0.23	4.287	58.282	5.078	32.123	-104564.1599	0.068722805
2	3363	0.578	10.784	60.441	5.266	22.931	-263032.4003	0.265833693
3	3439	1.004	18.733	63.082	5.496	11.685	-456916.3534	0.507086012
4	3477	1.221	22.784	64.428	5.613	5.955	-555724.2405	0.630047738
5	3497	1.331	24.848	65.113	5.673	3.034	-606067.237	0.692685163
6	3915	0.15	2.806	57.79	5.035	34.218	-68441.10862	0.0118559
7	4047	0.697	13.008	61.179	5.33	19.786	-317277.9547	0.320837135
8	4119	1.013	18.906	63.139	5.501	11.441	-461135.9941	0.499547264
9	4143	1.117	20.843	63.783	5.557	8.699	-508381.3353	0.558231929
10	4203	1.383	25.804	65.431	5.701	1.682	-629385.0202	0.70856143
11	4651	0.366	6.839	59.13	5.152	28.513	-166809.9579	0.121108228
12	4802	0.902	16.828	62.449	5.441	14.38	-410451.5238	0.423228294
13	4905	1.272	23.744	64.747	5.641	4.595	-579139.5877	0.632433785
14	4937	1.391	25.954	65.481	5.705	1.469	-633043.6682	0.699302387

Cellulose 45 kg/hr, Water 55 kg/hr, 25 C

		Organic Phase		Aqueous Phase			Enthalpy of Combustion in Organic Phase	
Run	Heat Duty	Water	HMF	Water	HMF	Cellulose	HMF	Q
	Cal/sec	Kg/hr	Kg/hr	Kg/hr	Kg/hr	Kg/hr	kJ/hr	
1	3555	57.861	10.015	0	0	32.123	-234113.4703	0.231435157
2	3813	2.575	9.626	57.329	7.538	22.931	-225020.0964	0.214799158
3	4124	4.912	18.354	57.491	7.558	11.685	-429048.291	0.47030129
4	4281	6.102	22.798	57.575	7.57	5.955	-532932.491	0.600420338
5	4361	6.706	25.062	57.62	7.578	3.034	-585856.3948	0.666709297
6	4126	57.396	3.186	0	0	34.218	-74476.8364	0.015802756
7	4549	3.228	12.067	57.374	7.544	19.786	-282081.6023	0.273726796
8	4792	4.962	18.543	57.495	7.558	11.441	-433466.4084	0.463067841
9	4871	5.529	20.669	57.537	7.565	8.699	-483164.3853	0.525241384
10	5072	6.986	26.111	57.64	7.581	1.682	-610378.1152	0.684412813
11	4965	1.417	5.296	57.247	7.528	28.513	-123800.7927	0.062824564
12	5398	4.353	16.263	57.452	7.552	14.38	-380168.4841	0.38305577
13	5694	6.383	23.851	57.596	7.574	4.595	-557547.7165	0.604691086
14	5789	7.03	26.276	57.644	7.581	1.469	-614235.2019	0.675514302

APPENDIX C.
ADDITIONAL RESOURCES

Data Used to Generate Figure 1.1 & Figure 1.2

	ΔH°_c (HHV) Kcal/gmole	ΔH°_f kJ/mol	Source
Xylan	-560.6		Wooley
Xylose	-561.5		Wooley
Cellulose	-671.9		Wooley
Glucose	-673		Wooley
CO_2 (*g*)		-393.52	NIST
H_2O (*l*)		-288.043	Wooley
Furfural (*l*)		-200.2	NIST
CO (*g*)		-110.53	NIST
CH_4 (*g*)		-74.87	NIST
Ethanol (*l*)		-276	NIST
HMF		-277.266	Benson

REFERENCES

ASPEN PLUS, version 23.0; Aspen Technology Inc.: MA, 2010.

Brown, R.L.; Stein , S.E., "Boiling Point Data" in **NIST Chemistry WebBook, NIST Standard Reference Database Number 69**, Eds. P.J. Linstrom and W.G. Mallard, National Institute of Standards and Technology, Gaithersburg MD, 20899, http://webbook.nist.gov, (retrieved November 3, 2012).

Domalski , E.S.; Hearing , E.D., "Condensed Phase Heat Capacity Data" in **NIST Chemistry WebBook, NIST Standard Reference Database Number 69**, Eds. P.J. Linstrom and W.G. Mallard, National Institute of Standards and Technology, Gaithersburg MD, 20899, http://webbook.nist.gov, (retrieved November 3, 2012).

Graboski, M. S. Fossil Energy Use in the Manufacture of Corn Ethanol: Prepared for National Corn Growers Association, 2002. http://www.oregon.gov/energy/RENEW/Biomass/docs/FORUM/FossilEnergyUse.pdf (accessed Nov 6, 2012).

Koretsky, M. D. *Engineering and Chemical Thermodynamics*; Wiley: Hoboken, NJ, 2004; pp 260.

Liquid-Liquid Equilibrium Data Collection Sørensen J. M.; Arlt, W.; Chemistry data series. v 5. Pt 2 Ternary systems [c1979-c1980]

Lorenz, D.; Morris, D., How Much Energy Does It Take to Make a Gallon of Ethanol, Institute for Local-Self Reliance, 1995.

Marrero-Morejón, J.; Pardillo-Fontdevilla, E. Estimation of Pure Compound Properties Using Group-Interaction Contributions. *AIChE J.*, **1999**, *45*, 615.

Petrus, L.; Voss, A. A Process for the Liquefaction of Lignocellulosic Material. World Intellectual Property Organization Patent WO 2005/058856 A1, 2005.

Pimentel, D.; Patzek, T. W. Ethanol Production Using Corn, Switchgrass, and Wood; Biodiesel Production Using Soybean and Sunflower. *Nat. Resour. Res. (Dordrecht, Neth.)* **2005**, *14*, 65-76.

Poling, B. E.; Prausnitz, J. M.; O'Connell, J. P. *The Properties of Gasses and Liquids*, 5^{th} ed; McGraw-Hill: New York, 2000.

Rackett, H. G. Equation of State for Saturated Liquids. *J. Chem. Eng. Data*. **1970**, *15*, 514-517.

Reid, R.C.; Poling, B. E.; Prausnitz, J. M. *The Properties of Gases and Liquids*, 4th ed; McGraw-Hill: New York, 1987.

Román-Leshkov, Y.; Barrett, C. J.; Liu, Z. Y.; Dumesic, J. A. Production of Dimethylfuran for Liquid Fuels from Biomas-Derived Carbohydrates. *Nature* (London, U. K.). **2007**, *447*, 982.

Seader, J. D.; Henley, E. J. *Separation Process Principles* 2nd ed; Wiley: Hoboken, NJ, 2006; pp 57.

Sokhansanj, S.; Turhollow, A.; Cushman, J.; Cundiff, J. Engineering Aspects of Collecting Corn Stover for Bioenergy. *Biomass Bioenergy*. **2002**, *23*, 347-355.

Kamm, B.; Gruber, P. R.; Kamm, M. *Biorefineries – Industrial Processes and Products*; Wiley-VCH: Weinheim, Germany, 2006; Vol. 1, pp 195.

Thermodynamics Research Center, NIST Boulder Laboratories, M. Frenkel director, "Thermodynamics Source Database" in **NIST Chemistry WebBook, NIST Standard Reference Database Number 69**, Eds. P.J. Linstrom and W.G. Mallard, National Institute of Standards and Technology, Gaithersburg MD, 20899, http://webbook.nist.gov, (retrieved November 3, 2012).

Wooley, R. J.; Putsche, V. *Development of an ASPEN PLUS Physical Property Database for Biofuels Components*; NREL/MP-425-20685; National Renewable Energy Laboratory: Golden, CO, 1996.

VITA

Zachary Daniel King was born in Lawrence, Kansas. He completed his Bachelor of Science degree in Chemical Engineering from the University of Kansas, Lawrence, Kansas in May 2007. He subsequently worked on data analysis and management of instrumentation for wind resource assessment projects, commencing graduate studies in 2009. He worked as an intern for NOWA Technology in the summer of 2010 at a pilot plant for converting wastewater sludge to useful biofuel feedstocks. He received his Master of Chemical Engineering degree from the Missouri University of Science and Technology, Rolla, Missouri in August 2014.